Edinburgh Research Explorer

Reducing Hypermuscularization of the Transitional Segment between Arterioles and Capillaries Protects Against Spontaneous Intracerebral Hemorrhage

1 **Reducing hypermuscularization of the transitional segment between**

2 **arterioles and capillaries protects against spontaneous intracerebral**

3 **hemorrhage**

4 **Short title: A novel mechanism of intracerebral hemorrhage**

5

6 **Authors**

7 Julien Ratelade, PhD, Nicholas R. Klug, PhD[#], Damiano Lombardi, PhD[#], Monara Kaelle

8 Servulo Cruz Angelim, PhD[#], Fabrice Dabertrand, PhD, Valérie Domenga-Denier, Rustam

9 Al-Shahi Salman, PhD, Colin Smith, MD, Jean-Frédéric Gerbeau, PhD, Mark T. Nelson,

10 PhD, Anne Joutel MD, PhD

11

12 # equal contribution

13 **Corresponding author**:

14 Anne Joutel, Inserm UMR 1266, Institute of Psychiatry and Neurosciences of Paris, 102-108

15 rue de la Santé, 75014 Paris, France

16

17 Email: anne.joutel@inserm.fr

18 Tel: +33 1 40 78 92 96

19

20 Text word counts (does not include title, abstract, ref, table, legends): 5151

21

ABSTRACT

Background: Spontaneous deep intracerebral hemorrhage (ICH) is a devastating subtype of stroke without specific treatments. It has been thought that smooth muscle cell (SMC) degeneration at the site of arteriolar wall rupture may be sufficient to cause hemorrhage. However, deep ICHs are rare in some aggressive small vessel diseases that are characterized by significant arteriolar SMC degeneration. Here we hypothesized that a second cellular defect may be required for the occurrence of ICH.

Methods: We studied a genetic model of spontaneous deep ICH using $Col4a1^{+/G498V}$ and $Col4a1^{+/G1064D}$ mouse lines that are mutated for the alpha1 chain of Collagen type IV. We performed high resolution imaging and molecular analyses of cerebroretinal microvessels, genetic rescue experiments, vascular reactivity analysis and computational modeling. We also examined post-mortem brain tissues from patients with sporadic deep ICH.

Results: We identified in the normal cerebroretinal vasculature a novel segment between arterioles and capillaries, herein called the transitional segment (TS), that is covered by mural cells distinct from SMCs and pericytes. In $Col4a1$ mutant mice, this TS was hypermuscularized, with a hyperplasia of mural cells expressing more contractile proteins, whereas the upstream arteriole exhibited a loss of SMCs. Mechanistically, TS showed a transient increase in proliferation of mural cells during post-natal maturation. Mutant brain microvessels, unlike mutant arteries, displayed a significant upregulation of SM genes and $Notch3$ target genes, and genetic reduction of $Notch3$ in $Col4a1^{+/G498V}$ mice protected against ICH. Retina analysis showed that hypermuscularization of the TS was attenuated but arteriolar SMC loss unchanged in $Col4a1^{+/G498V}$, $Notch3^{+/-}$ mice. Moreover, hypermuscularization of the retinal TS increased its contractility and tone and raised the intravascular pressure in the upstream feeding arteriole. Consistently, we similarly found

1 hypermuscularization of the TS and focal arteriolar SMC loss in brain tissues from patients

2 with sporadic deep ICH.

3 **Conclusions**: Our results suggest that hypermuscularization of the TS, via increased Notch3

4 activity, is involved in the occurrence of ICH in *Col4a1* mutant mice, by raising the

5 intravascular pressure in the upstream feeding arteriole and promoting its rupture at the site of

6 SMC loss. Our human data indicate that these 2 mutually reinforcing vascular defects may

7 represent a general mechanism of deep ICH.

8

9

1 **Clinical Perspective**

2 <u>What is new ?</u>

3 • *Col4a1* mutant mice, a genetic model of spontaneous deep intracerebral hemorrhage

4 (ICH), exhibit excessive muscularization of the transitional segment (TS) at the interface

5 between arterioles and capillaries, as a result of increased Notch3 activity, in addition to

6 focal loss of smooth muscle cells in arterioles, in the brain and the retina.

7 • Genetic reduction of *Notch3* in *Col4a1* mutant mice protects against ICH.

8 • Analysis of the retinal vasculature supports the concept of 2 mutually reinforcing vascular

9 defects as a mechanism of deep ICH, in which hypermuscularization of TS raises the

10 intravascular pressure in the upstream feeding arteriole crippled by smooth muscle cell

11 loss, and this ultimately leads to arteriolar rupture.

12 <u>What are the clinical implications?</u>

13 • Spontaneous ICH accounts for 10-20% of all strokes and is the most devastating subtype

14 of stroke, without specific treatments.

15 • Because these 2 mutually reinforcing vascular defects are present in the brain of patients

16 with sporadic deep ICH, this may represent a general mechanism of deep ICH and a

17 putative therapeutic target.

18

19

20

21

1 **INTRODUCTION**

2 Spontaneous (non-traumatic) intracerebral hemorrhage (ICH) accounts for 9-27% of all

3 strokes[1], causing about 3 million cases worldwide per year[2]. This stroke subtype is the most

4 devastating one because it is associated with high mortality rates (55% at one year) and major

5 permanent disabilities in patients who survive[3,4]. Cerebral small vessel diseases underlie the

6 vast majority of ICHs[5]: so-called hypertension-related arteriopathy accounts for almost all

7 deep ICH (occurring in the basal ganglia, thalamus, cerebellum or brainstem), whereas just

8 over half of lobar ICH is associated with cerebral amyloid angiopathy. Importantly, as

9 population blood pressure control has improved, epidemiological studies have found a

10 decreasing prevalence of uncontrolled hypertension at the time of ICH diagnosis[6,7], yet ICH

11 incidence appears unchanged[3].

12 Pathological studies on postmortem human brains have suggested that deep ICH results from

13 focal smooth muscle cell (SMC) degeneration in the media of cerebral arterioles and

14 replacement with collagen, which is structurally stiff and brittle[8–10]. It has been speculated that

15 the weakened arteriole dilates and eventually bursts at bifurcation sites and that this occurs

16 preferentially in deep brain regions where penetrating arterioles are exposed to high perfusion

17 pressure due to their proximity to the circle of Willis[11]. However, SMC loss alone may not be

18 sufficient to cause ICH because deep ICHs are rare in some aggressive small vessel diseases

19 that are characterized by significant arteriolar SMC degeneration[12]. Emerging evidence

20 indicates that mural cells exhibit a variety of cell phenotypes along the microvascular tree[13],

21 raising the possibility that mural cells may respond in different ways to the factors underlying

22 the arteriopathy.

23 Animal models of spontaneous deep ICHs are very rare. Beside sporadic forms of deep ICH,

24 monogenic forms largely indistinguishable from sporadic forms have been characterized

25 offering excellent opportunities for mechanistic studies using genetic models. Heterozygous

1   mutations in the α1 (COL4A1) chain of collagen type IV, which is a major component of

2   vascular basement membranes (BM), are associated with spontaneous deep ICHs in humans

3   or mice in the absence of hypertension, although with incomplete penetrance [14,15].

4   Herein, we hypothesized that a second cellular defect may be required for the occurrence of

5   ICH and we used *Col4a1* mutant mice to test this hypothesis.

6

1   **METHODS**

2   The data that support the findings of this study are available from the corresponding author

3   upon reasonable request.

4   *Human tissue samples*

5   Post-mortem frozen and paraffin embedded human brain samples were obtained from the UK

6   Medical Research Council Brain Bank of the University of Edinburgh, with informed consent

7   from patients or their families for their inclusion in the Lothian IntraCerebral Haemorrhage,

8   Pathology, Imaging and Neurological Outcome (LINCHPIN) study[5]. The use of postmortem

9   brain tissues for research was approved by the Institutional Review Board of INSERM

10   (IRB00003888, n°17-392).

11   *Mice*

12   $Col4a1^{+/G498V}$ mice used in this study were generated on a mixed 50% C57BL/6 – 50%

13   129/Sv background as described previously[14,16]. $Col4a1^{+/G1064D}$ mice on a C57BL/6

14   background were obtained from GlaxoSmithKline (Brentford, UK). $Notch3^{+/-}$ mice were

15   described previously[17]   and maintained on a 129/Sv background. All animals were

16   randomized for their genotype information and were included in the study. Mice were

17   maintained in a specific pathogen-free environment. Experiments were conducted in

18   accordance with the guidelines of our local institutional Animal Care and Use Committee

19   (Lariboisiere-Villemin, CEA9).

20   All other methods are described in the supplementary material.

21   *Statistical analysis*

22   Unless specified otherwise, data in figures and text are presented as means ± standard

23   deviation. Statistical significance was determined using either two-tailed Student's t-test, two-

24   tailed Mann-whitney test, one-way analysis of variance (ANOVA) followed by Tukey's post

25   hoc test, 2-way ANOVA followed by Bonferroni post hoc test or Kruskal-Wallis test followed

1   by Dunn's post hoc test, as specified in figure legends (GraphPad Prism 7 software). For large

2   samples (n>8), data were analyzed using parametric or non-parametric tests depending on the

3   result of the D'Agostino-Pearson omnibus normality test. Chi-square test was used to

4   compare the penetrance of ICHs between different groups.

5

1 **RESULTS**

2 *An unbiased, marker-based mural cell characterization of the retinal vasculature*

3 We focused on the superficial retinal vascular network that exhibits many similarities with the

4 cerebral vasculature and offers the advantage of being nearly planar on flat-mounted retina

5 preparations and highly stereotyped (Fig 1A). Moreover, we recently established the validity

6 of the retinal vasculature as a study model in the COL4A1 disease[14]. Flat-mounted retinas of

7 adult mice were stained for various mural cell markers including smooth muscle contractile

8 proteins —α smooth muscle actin (α-SMA) or smooth muscle myosin heavy chain

9 (SMMHC)—, the intermediate filament protein desmin, the plasma membrane chondroitin

10 sulfate proteoglycan (NG2), Platelet-derived growth factor receptor-beta (PDGFR-β), or

11 aminopetidase N (CD13). Markers of endothelial cells (VE-cadherin), astrocytes (GFAP,

12 aquaporin 4), BM (perlecan, COL4A2) or elastic lamina (elastin or Alexa Fluor 633–

13 conjugated hydrazide[18]) were also used. Arterioles (average diameter 26 µm) were surrounded

14 by $\alpha\text{-SMA}^{high}$, SMMHC^{high}, desmin^{low}, CD13^{low}, NG2^{low} and $\text{PDGFR-}\beta^{low}$ SMCs. Here,

15 SMCs had a flat ring-shape and were circumferentially organized in a perpendicular manner

16 towards the vessel axis (Figs 1B, S1 and S2). Veins (average diameter 32 µm) were

17 surrounded by stellate-shaped $\alpha\text{-SMA}^{low}$, SMMHC^{low}, desmin^{high}, CD13^{low}, NG2^{low} and

18 $\text{PDGFR-}\beta^{high}$ SMCs (Figs 1B, S1 and S2). Capillaries (average diameter 4.1 µm) were

19 covered by $\alpha\text{-SMA}^{negative}$, $\text{SMMHC}^{negative}$, desmin^{high}, CD13^{high}, NG2^{high} and $\text{PDGFR-}\beta^{high}$

20 mural cells, hereafter called pericytes, showing a protruding ovoid cell body ("bump on a

21 log") embedded in the BM, and elongated thin processes (Figs 1B, S1 and S2). Interestingly

22 the vascular segment located between arterioles and capillaries (average diameter 10 µm) was

23 covered by distinct mural cells, expressing both arteriolar SMC and pericyte markers. Namely

24 these cells were $\alpha\text{-SMA}^{high}$, SMMHC^{high}, desmin^{high}, CD13^{high}, NG2^{high} and $\text{PDGFR-}\beta^{high}$.

25 These mural cells had a pericyte-like protruding cell body, which contained the nucleus and

9

1   where NG2 staining was mostly concentrated (Fig S2B), but larger and irregular ensheathing

2   processes projecting orthogonally over the vessel, bright for α-SMA and SMMHC (Figs 1B,

3   S1 and S2). Thereafter, this vascular segment will be referred as "the transitional segment"

4   (TS) and its mural cells as "transitional cells". TS were present at every arteriole/capillary

5   transition, usually at the 1st-3rd branch orders (0 being the proximal arteriole starting in the

6   center of the retina) (Fig S3). Interestingly, TS, unlike arterioles, were devoid of elastic fibers

7   (Fig. S4C-D). On the other hand, expression of VE-cadherin, perlecan, COL4A2, GFAP and

8   aquaporin 4 was almost comparable along the arteriovenous bed (Fig. S4 and data not shown).

9   *Col4a1$^{+/G498V}$ mice have hypermuscularized TS in addition to arteriolar SMC loss in the*

10   *retinal vasculature*

11   Next, we studied microvascular changes in the retina of adult *Col4a1$^{+/G498V}$* mice (6-month-

12   old). Our previous work had shown segmental and focal loss and apoptosis of SMCs in the

13   retinal arterioles, starting from 3 months of age[14]. In keeping with this finding, we observed

14   that mural cell loss was strictly restricted to retinal arterioles and that remaining SMCs stained

15   negative for NG2 and low for desmin, suggesting that mutant SMCs have not undergone a

16   phenotypic switch towards a transitional cell or pericyte phenotype (Fig. S5). In striking

17   contrast, mutant TS exhibited a significantly higher number of mural cells with an increased

18   expression of contractile proteins including α-SMA or SMMHC (Fig. 2 A-C) that was already

19   present at one month of age (Fig S6), and we coined the term "hypermuscularization" to

20   designate these alterations. On the other hand, cell density and phenotype of pericytes were

21   unchanged in mutant capillaries although pericyte coverage was slightly increased (Fig. S7)

22   and no overt anomalies of SMCs were noticed in mutant veins.

23   To delineate the underlying cellular mechanisms of TS pathology, we examined whether there

24   was abnormal mural cell proliferation or apoptosis in mutant mice. The vascularization of the

25   murine retina occurs after birth and prior works suggest that mural cells are derived from a

1   common NG2+ precursor cell already present at birth[19,20]. At post-natal day 10 (P10),

2   arterioles were already easily recognizable as α-SMA bright vessels, yet SMCs were still

3   NG2 bright and had a protruding cell body, whereas TS just started to become discernable

4   (Figs 2D and S8). At P10, TS consisted in small branches covered by rounded mural cells that

5   were NG2 bright and α-SMA low-to-very pale (white-boxed area in Fig. 2D). We found that

6   the length and α-SMA expression level of TS were comparable between wildtype and mutant

7   mice (Fig. 2F). Incorporation of 5-ethynyl-2'-deoxyuridine (EdU) revealed a low number of

8   proliferating mural cells in TS, but which was significantly higher in $Col4a1^{+/G498V}$ mice (Fig.

9   2D-F). Very few apoptotic mural cells were present in TS in wildtype and mutant mice (Fig

10   S8D). At P23, TS had further grown and almost reached the adult mature state described

11   above. The length of TS was comparable between wildtype and mutant mice but α-SMA

12   expression level was significantly increased in mutant mice. Proliferating mural cells were no

13   longer detected and almost no apoptotic mural cells were observed in $Col4a1^{+/+}$ and

14   $Col4a1^{+/G498V}$ mice (Fig S8). SMC proliferation or apoptosis in arterioles was also very low at

15   P10 and P23, and notably comparable between wildtype and mutant mice (Fig. S8).

16   ***The brain vasculature of Col4a1^{+/G498V} and Col4a1^{+/G1064D} mutant mice display similar***

17   ***hypermuscularization of TS in addition to arteriolar SMC loss***

18   We next assessed whether the brain vasculature of *Col4a1* mutant mice displayed similar

19   changes to those of the retinal vasculature. Immunostaining of thick (100µm) brain slices

20   indicated that brain arterioles, like retinal arterioles, were surrounded by α-SMA^high ,

21   desmin^low and NG2^low SMCs, forming narrow circumferential bands, and brain TS were

22   surrounded by α-SMA^high , desmin^high and NG2^high mural cells having larger and irregular

23   ensheathing processes and a protruding cell body containing the nucleus wrapped by a bright

24   NG2 staining (Figs 3A-B and S9). Consistent with our previous work[14], we detected in

1 *Col4a1*[+/G498V] mice focal and segmental loss of SMCs in penetrating arterioles within regions

2 prone to ICH, like the thalamus (data not shown). Importantly, we found that α-SMA

3 expression in TS was significantly increased in *Col4a1*[+/G498V] mice compared to *Col4a1*^{+/+}

4 mice, not only in the thalamus but also in other brain regions, such as the cortex and striatum,

5 that are spared by ICH (Fig 3C-D).

6 The combination of arteriolar SMC loss and hypermuscularization of TS was similarly

7 observed in *Col4a1*[+/G1064D] mice, another independent *Col4a1* mutant line [21–23] in both the

8 retina and the brain, although vascular pathology was more severe than in *Col4a1*[+/G498V] mice

9 (expanded results, Figs S10-S11).

10 To understand the reason behind the differences between TS and arterioles in mutant mice,

11 and because Col4a1 mutations have been shown to decrease COL4 expression[14], we asked

12 whether COL4 expression levels were different between mutant arterioles and TS. Brain

13 cryosections (20μm-thick) of *Col4a1*^{+/+} and *Col4a1*[+/G498V] mice were immunostained with a

14 monoclonal antibody specific for COL4A2, which assembles with COL4A1 to form the

15 COL4A1A1A2 heterotrimer. Remarkably, COL4A2 immunoreactivity was significantly

16 decreased in mutant TS but unchanged in mutant arterioles (Fig. S12).

17 In the ensuing study, we focused on the role of the hypermuscularization of TS in ICH.

18

19 ***Expression of SMC genes and Notch3 target genes is upregulated in Col4a1*[+/G498V] *brain***

20 ***microvessel preparations enriched in TS***

21 To investigate molecular changes occurring in TS, we purified brain microvessels from

22 *Col4a1*^{+/+} and *Col4a1*[+/G498V] mice using sequential filtrations through nylon meshes of

23 decreasing pore sizes. Immunostaining of brain vessels retained on the 100 μm-nylon mesh

24 mainly comprised arterioles and veins (Fig 4A, top panel) whereas the 40 μm-retentate was

1   enriched in TS, and also in capillaries (Fig 4A, bottom panel). We found that genes coding for

2   the contractile proteins α-SMA and SMMHC were significantly upregulated in the TS

3   enriched fraction of *Col4a1$^{+/G498V}$* mice, as well as genes coding for desmin, the actin-binding

4   proteins calponin and SM22 and the transcription factor myocardin, suggesting an increased

5   differentiation of mural cells (Fig 4B).

6   The Notch3 receptor is predominantly expressed in vascular SMCs and Notch3 signaling

7   pathway plays a pivotal role in the development and maturation of blood vessels[24]. Moreover,

8   recent work suggests that activation of the Notch3 pathway promotes pulmonary arterial

9   hypertension by stimulating SMC proliferation and muscularization of small pulmonary

10   arteries[25]. Given these observations, and the finding that Notch3 is also expressed in

11   transitional cells (Fig. S13), we suspected that hypermuscularization of the TS could be

12   mediated by a dysregulation of the Notch3 pathway, and thus we quantified the expression of

13   target genes regulated by Notch3[26,27] (Supplementary table 1). Because our brain microvessel

14   preparations also contained endothelial cells, we selected Notch3 target genes that were

15   expressed exclusively in mural cells according to previous works[26,27] or single cell RNAseq

16   analysis of mouse brain microvessels

17   (*http://betsholtzlab.org/VascularSingleCells/database.html*) [13]. We found that 7 out of 11 of

18   these Notch3 target genes were upregulated in brain microvessels of *Col4a1$^{+/G498V}$* mice (Fig.

19   4C). In striking contrast, expression level of SM marker genes was essentially unchanged in

20   dissected brain arteries of *Col4a1$^{+/G498V}$* mice and only 2 out of 11 of Notch3 target genes

21   were upregulated in mutant brain arteries (Fig. 4D,E). Altogether, our results suggest that the

22   increased muscularization of mutant TS arises from an increased activation of Notch3

23   pathway.

24   ***Genetic reduction of Notch3 in Col4a1$^{+/G498V}$ mice attenuates the hypermuscularization of***

25   ***TS in the retina and protects against ICH***

1   To confirm that activation of the Notch3 pathway contributed to the hypermuscularization of

2   TS and assess whether this hypermuscularization was involved in ICH in *Col4a1* mutant

3   mice, we adopted a genetic interaction approach. To avoid confounding effects induced by the

4   complete loss of Notch3, which causes prominent loss of SMCs[17,28,29], we generated and

5   analyzed *Col4a1*[+/G498V] lacking 1 allele of Notch3, along with their control littermates, at 6

6   months of age. Loss of a single allele of Notch3 in wildtype mice (*Notch3*^{+/-}) has no

7   detectable morphological effect on the retinal microvasculature[29] but significantly reduces

8   Notch3 activity [26]. Genetic reduction of Notch3 in *Col4a1* mutant mice (*Col4a1*[+/G498V],

9   *Notch3*^{+/-}) had no significant effect on SMC loss in retinal arterioles (Fig. 5A,B), however, it

10   strikingly significantly attenuated α-SMA expression and mural cell number in TS (Fig

11   5C,D). Remarkably, the mean number of ICH was significantly reduced in *Col4a1*[+/G498V],

12   *Notch3*^{+/-} mice compared to *Col4a1*[+/G498V], *Notch3*^{+/+} mice (Fig 5E,F). Moreover, the

13   penetrance of ICH was drastically reduced in *Col4a1*[+/G498V], *Notch3*^{+/-} mice, with ICH being

14   detected in only 20% of mice compared to near 60% in the *Col4a1*[+/G498V], *Notch3*^{+/+} group

15   (P=0.024 by the Chi-square test)..

16   ***Mutant TS are more contractile in response to thromboxane receptor agonist and increased***

17   ***intraluminal pressure***

18   To pinpoint the mechanism by which hypermuscularization of the TS contributed to the

19   occurrence of ICH, we next performed functional studies. To achieve this, we used the retina

20   where TS can be easily identified *ex vivo* under phase contrast microscopy (Fig S3). To study

21   vascular responses closest to physiological conditions, we developed an *ex vivo* pressurized

22   retina preparation (Fig 6A). We assessed the response of TS to two standard vasoconstrictors,

23   KCl and the thromboxane mimetic U-46619 on retina explants from *Col4a1*^{+/+} and

24   *Col4a1*[+/G498V] mice aged 6 months (Fig. 6B and supplementary Table 2). Addition of 60 mM

25   KCl to the superfusion chamber elicited a robust and quick constriction of wildtype TS, with a

1 trend toward a stronger constriction in *Col4a1*[+/G498V] vessels (Fig S14). U-46619 (10-100nM)

2 produced a concentration-dependent constriction of TS that was significantly increased in

3 *Col4a1*[+/G498V] mice at 50 nM (36% diameter reduction in mutant mice versus 3% in control

4 mice) (Fig 6C,D). We also examined the contractile response of TS to increased intraluminal

5 pressure. Both *Col4a1*^{+/+} and *Col4a1*[+/G498V] TS decreased luminal diameter in response to the

6 pressure change, however *Col4a1*[+/G498V] TS exhibited a ~5.5-fold greater constriction than

7 *Col4a1*^{+/+} TS (Fig. 6E-F).

8 ***Hypermuscularization of the TS cripples the pressure drop in the microvasculature***

9 We then hypothesized that the higher tone and contractility of mutant TS could compromise

10 the pressure drop along the microvasculature. An abnormally higher intravascular pressure at

11 the level of arterioles combined with SMC loss might favor their rupture. Measuring

12 intravascular pressure *in vivo* in the microvasculature is extremely challenging and yet limited

13 to larger vessels. Moreover, assessing the pressure drop along the microvascular bed would

14 require several measurements at different locations which is not feasible *in vivo*. Therefore,

15 we used computational modeling to simulate the pressure distribution in different parts of the

16 microvasculature in the retina. We used an established mathematical model of an

17 artery/arteriolar human retinal network in which mural cells are implemented as fibers in the

18 vascular wall[30,31] (Fig. 7A). In *Col4a1* mutant mice, density of mural cells was decreased in

19 arterioles to model SMC loss and increased in TS to simulate the hypermuscularization (Fig.

20 7B). Measurements of systolic and diastolic blood pressures by tail-cuff plethysmography

21 showed a 11% decrease in *Col4a1* mutant mice (Fig. S15). Hence, blood pressures at the

22 entry of the retinal vascular network were decreased proportionally in *Col4a1* mutant mice

23 and used as input parameters for the model (Fig. 7B). Intravascular pressure was then

24 simulated in control and mutant mice all along the arterioles and TS (Fig. 7C). Fig 7D shows

25 the values of systolic and diastolic intravascular pressures in 10 different locations during a

1   typical cardiac cycle. In control mice, pressure continuously dropped from 40 to 20 mmHg. In

2   *Col4a1* mutant mice, a lower pressure was observed in proximal arterioles (positions 1-3) due

3   to the slight systemic hypotension. However, pressure drop was reduced resulting in higher

4   intravascular pressure in middle-size arterioles (positions 4-8) and TS (positions 9-10)

5   compared to controls. Moreover, in this part of the vascular network the pulse pressure

6   (difference between the systolic and diastolic pressure) was larger in *Col4a1* mutant mice.

7   Thus, these data suggest that the hypermuscularization of TS leads to an abnormally elevated

8   mean and pulse pressure in the feeding upstream arteriole.

9   ***Diffuse mural cell loss is not associated with ICH***

10   Our findings above predict that, conversely, loss of transitional cells in TS in addition to SMC

11   loss in arterioles should not lead to ICH (Fig. 7E). Consistent with previous reports[17,28,29],

12   cerebral and retinal arterioles of mice completely lacking *Notch3* exhibited prominent SMC

13   loss (Figs S16-S17). However, unlike *Col4a1* mutant mice, we found that TS in *Notch3*^{-/-}

14   mice also showed dramatic loss of transitional cells in both the retina and the brain (Figs S16-

15   S17). Computational modeling revealed that arterioles in *Notch3*^{-/-} mice were exposed to

16   lower intravascular pressure compared to controls (Fig. 7C,D). Remarkably, Perl's staining

17   revealed no ICH in *Notch3*^{-/-} mice aged 10-12 months (Fig. S17).

18   ***Cerebral TS are hypermuscularized in humans with sporadic deep ICH***

19   Finally, we tested if hypermuscularization of TS was also present in humans with sporadic

20   ICH. Similarly to murine cerebral vessels, human cerebral arteries were surrounded by flat

21   ring-shaped SMCs whereas α-SMA positive smaller vessels (diameter between 5 and 15 μm)

22   were covered by mural cells having a protruding ovoid cell body (Fig. S18). These vessels are

23   most likely TS, although transitional cells could not be further characterized because none of

24   the antibodies against NG2, desmin or aminopeptidase N worked on human post-mortem

16

brain tissue in our experimental conditions. To assess vascular remodeling in human deep

ICH, we immunostained for α-SMA paraffin sections of postmortem brain tissues from adults

who suffered from spontaneous deep ICH (Fig. 8A) and age and sex-matched control subjects

(Supplementary table 3). To ensure that vascular lesions were not secondary to ICH, we used

tissue sampled in the hemisphere contralateral to the hemorrhage, and we analyzed sections

through the basal ganglia. In agreement to what has been previously reported[8], we observed

that some, but not all, arteries in patients had a markedly reduced α-SMA staining in the

media with an uneven distribution of stained SMC, consistent with segmental and focal SMC

degeneration (Fig. S19). In contrast, TS in ICH patients often showed a marked increased

immunostaining for α-SMA compared to controls, suggesting an increased number or

hypertrophy of mural cells (Fig 8B). We imaged cross-sectional profiles of 525 randomly

selected TS/arterioles in patients and controls. Quantification of the ratio of the area stained

for α-SMA (media) over the area of the lumen confirmed that α-SMA staining was

significantly thicker in TS (lumen diameter between 5 and 15 µm) from ICH patients whereas

α-SMA staining in arterioles (lumen diameter > 15µm) was comparable between ICH patients

and controls (Fig. 8C-D). Overall, our data suggest that hypermuscularization of TS is a

common pathological mechanism in spontaneous deep ICH.

DISCUSSION

In the present study, we investigated the microvascular pathology in mice mutant for collagen type IV, a model of hereditary spontaneous deep ICH, and provided strong experimental evidence for two mutually-reinforcing defects of the brain microvasculature as a new mechanism for ICH. In our previous study, we had demonstrated that ICH originate from deep brain arteries with focal and segmental loss of SMC[14]. In the present study, we demonstrate that TS, the downstream microvessels at the interface between arteries and capillaries, show an exaggerated muscularization with higher contractility and tone. Our data support a mechanism in which hypermuscularization of mutant TS is driven by increased Notch3 activity, cripples the pressure drop along the arterio-capillary axis, raising the intravascular pressure in the upstream feeding arteriole and promoting its rupture at the site of SMC loss (Fig. 7E). We found similar microvascular lesions in post mortem brain tissues from patients with sporadic deep ICH, indicating that this may represent a general mechanism of deep ICH.

Zonation of microvascular pathology in Col4a1-related small vessel disease

Several groups have highlighted the diversity of mural cells in the brain microvasculature as arterioles branch into capillaries based on cellular morphology, α-SMA content or vascular territory[32,33]. Recently, Vanlandewijck, He and colleagues proposed the concept of mural cell zonation, by which these cells can be grouped in distinct populations according to their gene repertoire[13]. Herein, we took advantage of the flat mounted retina preparation, in which the arteriovenous axis can be observed in a single plane, to precisely define the phenotype of mural cells at the arteriole-capillary interface, by using a combination of several mural cell markers and high-resolution imaging. Consistent with recent reports[32,33], we found that

1   microvessels at the interface between arterioles and capillaries (mean diameter 10 μm), herein

2   called TS, are covered by a population of mural cells that are distinct from the canonical ring-

3   shaped α-SMA positive SMCs located in arterioles and arteries, and the canonical α-SMA

4   negative pericytes, which have a protruding cell body and extend thin and long processes

5   along the capillaries. We further established that these mural cells robustly express markers of

6   both canonical SMCs and pericytes and extend large and short processes but have a

7   protruding cell body. We then demonstrated the presence of similar transitional cells in the

8   cerebral vessels. We believe that the name of transitional cell, rather than "contractile

9   pericyte" [34,35], "ensheathing pericyte"[32] or "pre-capillary SMC"[33] better reflects the similarity

10   and the continuum between these mural cells and the adjacent canonical SMCs and pericytes.

11   Remarkably, the zonation of mural cells, as described above, coincides with the zonation

12   of microvascular pathology in *Col4a1* mutant mice. Notably, our time course, cellular,

13   molecular and genetic experiments strongly suggest that the exaggerated muscularization of

14   the TS and arteriolar SMC loss are driven by different mechanisms.

15

16   **Mechanism of excessive muscularization of TS in *Col4a1* mutant mice**

17   Increased α-SMA expression and mural cell numbers in TS include several possible

18   underlying mechanisms. Analysis of the retinal vasculature at P10, the earliest time point

19   when TS were discernable, revealed that proliferation of mural cells, although low, was

20   transiently increased in mutant TS. While the increased number of transitional cells may

21   largely contribute to the increased expression of SM contractile proteins, our finding of an

22   upregulation of several SM genes including myocardin, a transcription factor critically

23   involved in SMC differentiation, is consistent with an enhanced differentiation of transitional

24   cells in mutant TS— noting that we did not find evidence of a premature differentiation of

25   these cells.

19

1   Our findings that Notch3 target genes were upregulated in mutant brain microvessels

2   and that hypermuscularization of retinal TS in *Col4a1*[+/G498V] mice was attenuated by genetic

3   reduction of Notch3, suggest that increased Notch3 activity is a driver of TS pathology. This

4   conclusion is consistent with a number of previous studies that clearly established a pivotal

5   role of Notch3 on early mural cell specification, differentiation and expression of SMC

6   genes[17,28,29,36–38]. It is also worth mentioning that Notch3 has been identified as a mediator of

7   SMC proliferation and muscularization of small pulmonary arteries in the context of

8   pulmonary hypertension[25]. Considering a recent report showing that COL4 can repress

9   Notch3 signaling[39], it is plausible that the reduction in COL4 expression in mutant TS could

10   be involved in this increased Notch3 activity. Nevertheless, further studies are warranted to

11   better understand the mechanisms by which Col4a1 mutations increase Notch3 activity in

12   mutant TS and of Notch3-mediated hypermuscularization of mutant TS. In this regard, it will

13   be critical to better understand the molecular and physiological factors that underlie the

14   differentiation of mural cells in transitional or arteriolar vessels. However, one current

15   limitation is the absence of specific marker or genetically encoded reporter of transitional

16   cells.

17

18   **Why TS respond to Col4a1 mutations with hypermuscularization whereas arteries do**

19   **not?**

20   We found that arteries differed from TS in several respects. Notably, Col4a1 mutation did not

21   affect expression of COL4 and marginally affected expression of Notch3 target genes in

22   mutant arteries. This different response of arterial SMCs and transitional cells to Col4a1

23   mutation may originate from their distinct intrinsic molecular identity highlighted in this

24   study. Furthermore, the distinct environment of SMCs in arterioles compared to mural cells in

25   transitional segments offers an additional possible explanation. Indeed, communication

between endothelial cells and SMCs in arteries is hampered by the presence of an internal

elastic lamina which restricts cell-cell communication to myoendothelial projections [40]. In

contrast, endothelial cells are in direct contact with transitional cells in TS, which are devoid

of elastic lamina. Thus, the distinct pathology of arteriolar SMCs and transitional cells in

Col4a1 mutant mice may arise from cell autonomous effects versus endothelial cell-mediated,

i.e. non-cell autonomous, effects respectively[41]. Future work is needed to investigate this

hypothesis.

Two mutually-reinforcing defects of the brain microvasculature as a key mechanism for

spontaneous deep ICH

We recently reported that *Col4a1* mutant mice exhibited arteriolar SMC loss in the brain

and the retina, and that ICH originated from arterioles with severe loss of SMC[14]. In this

study, we demonstrated that mutant TS in the brain and the retina were hypermuscularized.

Our Notch3 genetic reduction experiment in *Col4a1* mutant mice further suggests that

hypermuscularization of the TS plays a role in the occurrence of ICH. By analyzing the retina,

which is a tractable central nervous system preparation where vessels of the superficial layer

are at similar depths and can be easily fully imaged, we demonstrated that

hypermuscularization of TS was attenuated and arteriolar SMC loss unchanged in *Col4a1*

mutant mice haploinsufficient for *Notch3*. Remarkably, these mice were protected against

hemorrhage. Additional studies would be desirable to confirm that hypermuscularization of

TS is similarly attenuated and arteriolar SMC loss similarly unchanged in the brain of *Col4a1*

compound heterozygotes, although such quantifications are still extremely challenging

because the cerebral vasculature spans several spatial scales and forms a highly complex

network. Moreover, our demonstration in Notch3 null mice that a severe loss of mural cells in

both arterioles and TS does not necessarily lead to ICHs, lends further support to the concept

1 that the hypermuscularization of TS in addition to arteriolar SMC loss is involved in ICH

2 occurrence.

3   Hypermuscularization of TS is predicted to locally decrease vessel diameter, increase

4 vascular resistance and raise the intravascular pressure in the upstream proximate arteriole,

5 hence favoring its rupture at the site of SMC loss. Both our experimental data and our

6 computational modeling support these predictions. First, using our pressurized retina

7 preparation, we found that pressure increase caused a significantly higher reduction in the

8 diameter of TS in *Col4a1* mutant mice compared to control mice. Second, our computational

9 modeling revealed that the pressure drop along the arterio-TS axis was crippled in *Col4a1*

10 mutant mice, ie with an abnormally higher intravascular pressure in the proximate feeding

11 arteriole, despite the fact that *Col4a1* mutant mice were slightly hypotensive. Notably, our

12 computational modeling approach showed that arterioles in *Notch3* null mice were instead

13 exposed to lower intravascular pressure, which likely protected them against rupture and

14 hemorrhage as observed experimentally.

15   ICHs in *Col4a1* mutant mice preferentially occur in the deep parts of the brain. This

16 anatomical specificity of ICH is likely attributed in part to the following factors. First, in a

17 previous study, we reported that arteriolar SMC loss predominated in the deep penetrating

18 arteries[14]. Secondly, although hypermuscularization of TS is not restricted to ICH prone

19 regions, the mechanism by which it favors arteriolar rupture, namely by raising the

20 intravascular pressure at the site of SMC loss, suggests that it could contribute to the regional

21 specificity of ICH. Indeed, recent computational modeling in human suggests that

22 intravascular pressure at the level of perforating arteries in the deep parts of the brain is higher

23 than the one at the level of penetrating arteries in the cortex, owing to their anatomical

24 proximity to the circle of Willis[42]. Therefore, it is anticipated that it is in those deep

1   penetrating arteries that hypermuscularization of TS should produce the highest local

2   elevation of intravascular pressure.

3

4   **Excessive muscularization of the TS in sporadic deep ICH**

5   In patients with sporadic deep ICH, SMC degeneration has been documented at the

6   presumed site of arterial wall rupture for many years[10,11]. So far, the assumption has been

7   made that vessel wall degeneration was uniquely responsible for bleeding. Our findings in

8   *Col4a1* mutant mice, a genetic model of spontaneous deep ICH, prompted us to test the

9   possibility that sporadic deep ICH in humans may also arise from a similar zonation of

10   microvascular pathology. Remarkably, analysis of human post-mortem brain tissues from

11   patients with spontaneous deep ICH revealed, in addition to segmental SMC degeneration in

12   arteries, a thickening of α-SMA staining in smaller vessels, consistent with a hyperplasia or

13   hypertrophy of mural cells. Although, we could not unequivocally identify these vessels as TS

14   because most of the mural cell markers used in the mouse did not work on human tissues in

15   our experimental conditions, the presence of protruding cell nuclei and the internal diameter

16   of the affected vessels, comprised between 5-15 μm, strongly suggest that these are TS.

17   Hence our data suggest that the mechanism of ICH identified in *Col4a1* mutant mice also

18   operates in human sporadic deep ICH. Yet, whether Notch3 activity is similarly increased in

19   TS in patients needs to be further investigated.

20   Our findings open new opportunities towards the development of preventive therapies

21   for ICH. Although several studies have established the benefit of blood pressure lowering in

22   preventing the recurrence of ICH (secondary prevention) [43–45], our data suggest that

23   pharmacological compounds targeting hypermuscularization of the TS may be more effective

24   for both primary and secondary prevention of ICH. Notably, hypermuscularization of the TS

25   may prove to be more easily druggable than arteriolar SMC loss.

Conclusion

Collectively our work is consistent with the new concept of two mutually-reinforcing defects of the brain microvasculature, with arteriolar SMC loss and exaggerated muscularization of the TS, as a new mechanism underlying hereditary and sporadic deep ICH. Hypermuscularization of this segment may represent a novel therapeutic target for ICH prevention.

20

21 **DISCLOSURES**

22 None.

23

24 **SUPPLEMENTAL MATERIALS**

25 Expanded Material & Methods

1   Online Figures 1-19

2   Online Tables I-III

3   References 46-51

4

5   **AFFILIATIONS**

6   From Institute of Psychiatry and Neurosciences of Paris, INSERM UMR1266, Paris Descartes

7   University, Paris, France (JR, VDD, MKSCA, AJ); Department of Pharmacology, College of

8   Medicine, University of Vermont, Burlington, VT, USA (NK, FD, MTN, AJ); Inria Paris,

9   Sorbonne Université, Laboratoire Jacques-Louis Lions, Paris, France (DL, JFG) ; Centre for

10   Clinical Brain Sciences, University of Edinburgh, Edinburgh, UK (RA-SS, CS); Division of

11   Cardiovascular Sciences, University of Manchester, Manchester, UK (MTN); DHU

12   NeuroVasc, Sorbonne Paris Cité, Paris, France (AJ)

13   # Equal contribution (DL, NK, MKSCA)

14

15

16

REFERENCES

1. Feigin VL, Lawes CMM, Bennett DA, Barker-Collo SL, Parag V. Worldwide stroke incidence and early case fatality reported in 56 population-based studies: a systematic review. *Lancet Neurol*. 2009;8:355–369.

2. Feigin VL, Krishnamurthi RV, Parmar P, Norrving B, Mensah GA, Bennett DA, Barker-Collo S, Moran AE, Sacco RL, Truelsen T, Davis S, Pandian JD, Naghavi M, Forouzanfar MH, Nguyen G, Johnson CO, Vos T, Meretoja A, Murray CJL, Roth GA, GBD 2013 Writing Group, GBD 2013 Stroke Panel Experts Group. Update on the Global Burden of Ischemic and Hemorrhagic Stroke in 1990-2013: The GBD 2013 Study. *Neuroepidemiology*. 2015;45:161–176.

3. van Asch CJ, Luitse MJ, Rinkel GJ, van der Tweel I, Algra A, Klijn CJ. Incidence, case fatality, and functional outcome of intracerebral haemorrhage over time, according to age, sex, and ethnic origin: a systematic review and meta-analysis. *Lancet Neurol*. 2010;9:167–176.

4. Cordonnier C, Demchuk A, Ziai W, Anderson CS. Intracerebral haemorrhage: current approaches to acute management. *Lancet*. 2018;392:1257–1268.

5. Rodrigues MA, Samarasekera N, Lerpiniere C, Humphreys C, McCarron MO, White PM, Nicoll JAR, Sudlow CLM, Cordonnier C, Wardlaw JM, Smith C, Al-Shahi Salman R. The Edinburgh CT and genetic diagnostic criteria for lobar intracerebral haemorrhage associated with cerebral amyloid angiopathy: model development and diagnostic test accuracy study. *Lancet Neurol*. 2018;17:232–240.

6. Lovelock CE, Molyneux AJ, Rothwell PM, Oxford Vascular Study. Change in incidence and aetiology of intracerebral haemorrhage in Oxfordshire, UK, between 1981 and 2006: a population-based study. *Lancet Neurol*. 2007;6:487–493.

7. Samarasekera N, Fonville A, Lerpiniere C, Farrall AJ, Wardlaw JM, White PM, Smith C, Al-Shahi Salman R, Lothian Audit of the Treatment of Cerebral Haemorrhage Collaborators. Influence of intracerebral hemorrhage location on incidence, characteristics, and outcome: population-based study. *Stroke*. 2015;46:361–368.

8. Sutherland GR, Auer RN. Primary intracerebral hemorrhage. *J Clin Neurosci*. 2006;13:511–517.

9. Masawa N, Yoshida Y, Yamada T, Joshita T, Sato S, Mihara B. Morphometry of structural preservation of tunica media in aged and hypertensive human intracerebral arteries. *Stroke*. 1994;25:122–127.

10. Takebayashi S, Kaneko M. Electron microscopic studies of ruptured arteries in hypertensive intracerebral hemorrhage. *Stroke*. 1983;14:28–36.

11. Schlunk F, Greenberg SM. The Pathophysiology of Intracerebral Hemorrhage Formation and Expansion. *Transl Stroke Res*. 2015;6:257–263.

27

1 12. Chabriat H, Joutel A, Dichgans M, Tournier-Lasserve E, Bousser M-G. Cadasil. *Lancet*
2   *Neurol*. 2009;8:643–653.

3 13. Vanlandewijck M, He L, Mäe MA, Andrae J, Ando K, Del Gaudio F, Nahar K,
4   Lebouvier T, Laviña B, Gouveia L, Sun Y, Raschperger E, Räsänen M, Zarb Y,
5   Mochizuki N, Keller A, Lendahl U, Betsholtz C. A molecular atlas of cell types and
6   zonation in the brain vasculature. *Nature*. 2018;554:475–480.

7 14. Ratelade J, Mezouar N, Domenga-Denier V, Rochey A, Plaisier E, Joutel A. Severity of
8   arterial defects in the retina correlates with the burden of intracerebral haemorrhage in
9   COL4A1-related stroke. *J Pathol*. 2018;244:408–420.

10 15. Kuo DS, Labelle-Dumais C, Gould DB. COL4A1 and COL4A2 mutations and disease:
11   insights into pathogenic mechanisms and potential therapeutic targets. *Hum Mol Genet*.
12   2012;21:R97-110.

13 16. Chen Z, Migeon T, Verpont M-C, Zaidan M, Sado Y, Kerjaschki D, Ronco P, Plaisier E.
14   HANAC Syndrome Col4a1 Mutation Causes Neonate Glomerular Hyperpermeability
15   and Adult Glomerulocystic Kidney Disease. *J Am Soc Nephrol*. 2016;27:1042–1054.

16 17. Domenga V, Fardoux P, Lacombe P, Monet M, Maciazek J, Krebs LT, Klonjkowski B,
17   Berrou E, Mericskay M, Li Z, Tournier-Lasserve E, Gridley T, Joutel A. Notch3 is
18   required for arterial identity and maturation of vascular smooth muscle cells. *Genes Dev*.
19   2004;18:2730–5.

20 18. Shen Z, Lu Z, Chhatbar PY, O'Herron P, Kara P. An artery-specific fluorescent dye for
21   studying neurovascular coupling. *Nat Methods*. 2012;9:273–276.

22 19. Hughes S, Chan-Ling T. Characterization of smooth muscle cell and pericyte
23   differentiation in the rat retina in vivo. *Invest Ophthalmol Vis Sci*. 2004;45:2795–2806.

24 20. Ehling M, Adams S, Benedito R, Adams RH. Notch controls retinal blood vessel
25   maturation and quiescence. *Development*. 2013;140:3051–3061.

26 21. Van Agtmael T, Schlötzer-Schrehardt U, McKie L, Brownstein DG, Lee AW, Cross SH,
27   Sado Y, Mullins JJ, Pöschl E, Jackson IJ. Dominant mutations of Col4a1 result in
28   basement membrane defects which lead to anterior segment dysgenesis and
29   glomerulopathy. *Hum Mol Genet*. 2005;14:3161–3168.

30 22. Jones FE, Bailey MA, Murray LS, Lu Y, McNeilly S, Schlötzer-Schrehardt U, Lennon
31   R, Sado Y, Brownstein DG, Mullins JJ, Kadler KE, Van Agtmael T. ER stress and
32   basement membrane defects combine to cause glomerular and tubular renal disease
33   resulting from Col4a1 mutations in mice. *Dis Model Mech*. 2016;9:165–176.

34 23. Jones FE, Murray LS, McNeilly S, Dean A, Aman A, Lu Y, Nikolova N, Malomgré R,
35   Horsburgh K, Holmes WM, Kadler KE, Van Agtmael T. 4-Sodium phenyl butyric acid
36   has both efficacy and counter-indicative effects in the treatment of Col4a1 disease. *Hum*
37   *Mol Genet*. 2019;28:628–638.

38 24. Baeten JT, Lilly B. Notch Signaling in Vascular Smooth Muscle Cells. *Adv Pharmacol*.
39   2017;78:351–382.

25. Li X, Zhang X, Leathers R, Makino A, Huang C, Parsa P, Macias J, Yuan JX-J, Jamieson SW, Thistlethwaite PA. Notch3 signaling promotes the development of pulmonary arterial hypertension. *Nat Med*. 2009;15:1289–1297.

26. Cognat E, Baron-Menguy C, Domenga-Denier V, Cleophax S, Fouillade C, Monet-Leprêtre M, Dewerchin M, Joutel A. Archetypal Arg169Cys mutation in NOTCH3 does not drive the pathogenesis in cerebral autosomal dominant arteriopathy with subcortical infarcts and leucoencephalopathy via a loss-of-function mechanism. *Stroke*. 2014;45:842–849.

27. Fouillade C, Baron-Menguy C, Domenga-Denier V, Thibault C, Takamiya K, Huganir R, Joutel A. Transcriptome analysis for Notch3 target genes identifies Grip2 as a novel regulator of myogenic response in the cerebrovasculature. *Arterioscler Thromb Vasc Biol*. 2013;33:76–86.

28. Liu H, Zhang W, Kennard S, Caldwell RB, Lilly B. Notch3 is critical for proper angiogenesis and mural cell investment. *Circ Res*. 2010;107:860–70.

29. Henshall TL, Keller A, He L, Johansson BR, Wallgard E, Raschperger E, Mäe MA, Jin S, Betsholtz C, Lendahl U. Notch3 is necessary for blood vessel integrity in the central nervous system. *Arterioscler Thromb Vasc Biol*. 2015;35:409–420.

30. Aletti M, Gerbeau J-F, Lombardi D. A simplified fluid-structure model for arterial flow. Application to retinal hemodynamics. *Computational Methods in Applied Mechanics and Engineering*. 2016;306:77–94.

31. Aletti M, Gerbeau J-F, Lombardi D. Modeling autoregulation in three-dimensional simulations of retinal hemodynamics. *Journal for Modeling in Ophthalmology*. 2016;1:88–115.

32. Grant RI, Hartmann DA, Underly RG, Berthiaume A-A, Bhat NR, Shih AY. Organizational hierarchy and structural diversity of microvascular pericytes in adult mouse cortex. *J Cereb Blood Flow Metab*. 2017;271678X17732229.

33. Hill RA, Tong L, Yuan P, Murikinati S, Gupta S, Grutzendler J. Regional Blood Flow in the Normal and Ischemic Brain Is Controlled by Arteriolar Smooth Muscle Cell Contractility and Not by Capillary Pericytes. *Neuron*. 2015;87:95–110.

34. Attwell D, Mishra A, Hall CN, O'Farrell FM, Dalkara T. What is a pericyte? *J Cereb Blood Flow Metab*. 2016;36:451–455.

35. Hall CN, Reynell C, Gesslein B, Hamilton NB, Mishra A, Sutherland BA, O'Farrell FM, Buchan AM, Lauritzen M, Attwell D. Capillary pericytes regulate cerebral blood flow in health and disease. *Nature*. 2014;508:55–60.

36. Doi H, Iso T, Sato H, Yamazaki M, Matsui H, Tanaka T, Manabe I, Arai M, Nagai R, Kurabayashi M. Jagged1-selective notch signaling induces smooth muscle differentiation via a RBP-Jkappa-dependent pathway. *J Biol Chem*. 2006;281:28555–28564.

1   37. Granata A, Bernard WG, Zhao N, Mccafferty J, Lilly B, Sinha S. Temporal and
2   embryonic lineage-dependent regulation of human vascular SMC development by
3   NOTCH3. *Stem Cells Dev*. 2015;24:846–856.

4   38. Ando K, Wang W, Peng D, Chiba A, Lagendijk AK, Barske L, Crump JG, Stainier
5   DYR, Lendahl U, Koltowska K, Hogan BM, Fukuhara S, Mochizuki N, Betsholtz C.
6   Peri-arterial specification of vascular mural cells from naïve mesenchyme requires
7   Notch signaling. *Development*. 2019;146.

8   39. Zhang X, Meng H, Wang MM. Collagen represses canonical Notch signaling and binds
9   to Notch ectodomain. *Int J Biochem Cell Biol*. 2013;45:1274–1280.

10   40. Sandow SL, Gzik DJ, Lee RMKW. Arterial internal elastic lamina holes: relationship to
11   function? *J Anat*. 2009;214:258–266.

12   41. Sheikh AQ, Saddouk FZ, Ntokou A, Mazurek R, Greif DM. Cell Autonomous and Non-
13   cell Autonomous Regulation of SMC Progenitors in Pulmonary Hypertension. *Cell Rep*.
14   2018;23:1152–1165.

15   42. Blanco PJ, Müller LO, Spence JD. Blood pressure gradients in cerebral arteries: a clue to
16   pathogenesis of cerebral small vessel disease. *Stroke Vasc Neurol*. 2017;2:108–117.

17   43. Biffi A, Anderson CD, Battey TWK, Ayres AM, Greenberg SM, Viswanathan A,
18   Rosand J. Association Between Blood Pressure Control and Risk of Recurrent
19   Intracerebral Hemorrhage. *JAMA*. 2015;314:904–912.

20   44. PROGRESS Collaborative Group. Randomised trial of a perindopril-based blood-
21   pressure-lowering regimen among 6,105 individuals with previous stroke or transient
22   ischaemic attack. *Lancet*. 2001;358:1033–1041.

23   45. SPS3 Study Group, Benavente OR, Coffey CS, Conwit R, Hart RG, McClure LA,
24   Pearce LA, Pergola PE, Szychowski JM. Blood-pressure targets in patients with recent
25   lacunar stroke: the SPS3 randomised trial. *Lancet*. 2013;382:507–515.

26   46. Khoshnoodi J, Pedchenko V, Hudson BG. Mammalian collagen IV. *Microsc Res Tech*.
27   2008;71:357–370.

28   47. Chen Z-L, Yao Y, Norris EH, Kruyer A, Jno-Charles O, Akhmerov A, Strickland S.
29   Ablation of astrocytic laminin impairs vascular smooth muscle cell function and leads to
30   hemorrhagic stroke. *J Cell Biol*. 2013;202:381–395.

31   48. Yao Y, Chen Z-L, Norris EH, Strickland S. Astrocytic laminin regulates pericyte
32   differentiation and maintains blood brain barrier integrity. *Nat Commun*. 2014;5:3413.

33   49. De Silva TM, Faraci FM. Microvascular Dysfunction and Cognitive Impairment. *Cell*
34   *Mol Neurobiol*. 2016;36:241–258.

35   50. Rannikmäe K, Davies G, Thomson PA, Bevan S, Devan WJ, Falcone GJ, Traylor M,
36   Anderson CD, Battey TWK, Radmanesh F, Deka R, Woo JG, Martin LJ, Jimenez-Conde
37   J, Selim M, Brown DL, Silliman SL, Kidwell CS, Montaner J, Langefeld CD, Slowik A,
38   Hansen BM, Lindgren AG, Meschia JF, Fornage M, Bis JC, Debette S, Ikram MA,
39   Longstreth WT, Schmidt R, Zhang CR, Yang Q, Sharma P, Kittner SJ, Mitchell BD,

1   Holliday EG, Levi CR, Attia J, Rothwell PM, Poole DL, Boncoraglio GB, Psaty BM,
2   Malik R, Rost N, Worrall BB, Dichgans M, Van Agtmael T, Woo D, Markus HS,
3   Seshadri S, Rosand J, Sudlow CLM, METASTROKE Consortium, CHARGE WMH
4   Group, ISGC ICH GWAS Study Collaboration, WMH in Ischemic Stroke GWAS Study
5   Collaboration, International Stroke Genetics Consortium. Common variation in
6   COL4A1/COL4A2 is associated with sporadic cerebral small vessel disease. *Neurology*.
7   2015;84:918–926.

8   51. Rannikmäe K, Sivakumaran V, Millar H, Malik R, Anderson CD, Chong M, Dave T,
9   Falcone GJ, Fernandez-Cadenas I, Jimenez-Conde J, Lindgren A, Montaner J,
10   O'Donnell M, Paré G, Radmanesh F, Rost NS, Slowik A, Söderholm M, Traylor M,
11   Pulit SL, Seshadri S, Worrall BB, Woo D, Markus HS, Mitchell BD, Dichgans M,
12   Rosand J, Sudlow CLM, Stroke Genetics Network (SiGN), METASTROKE
13   Collaboration, and International Stroke Genetics Consortium (ISGC). COL4A2 is
14   associated with lacunar ischemic stroke and deep ICH: Meta-analyses among 21,500
15   cases and 40,600 controls. *Neurology*. 2017;89:1829–1839.
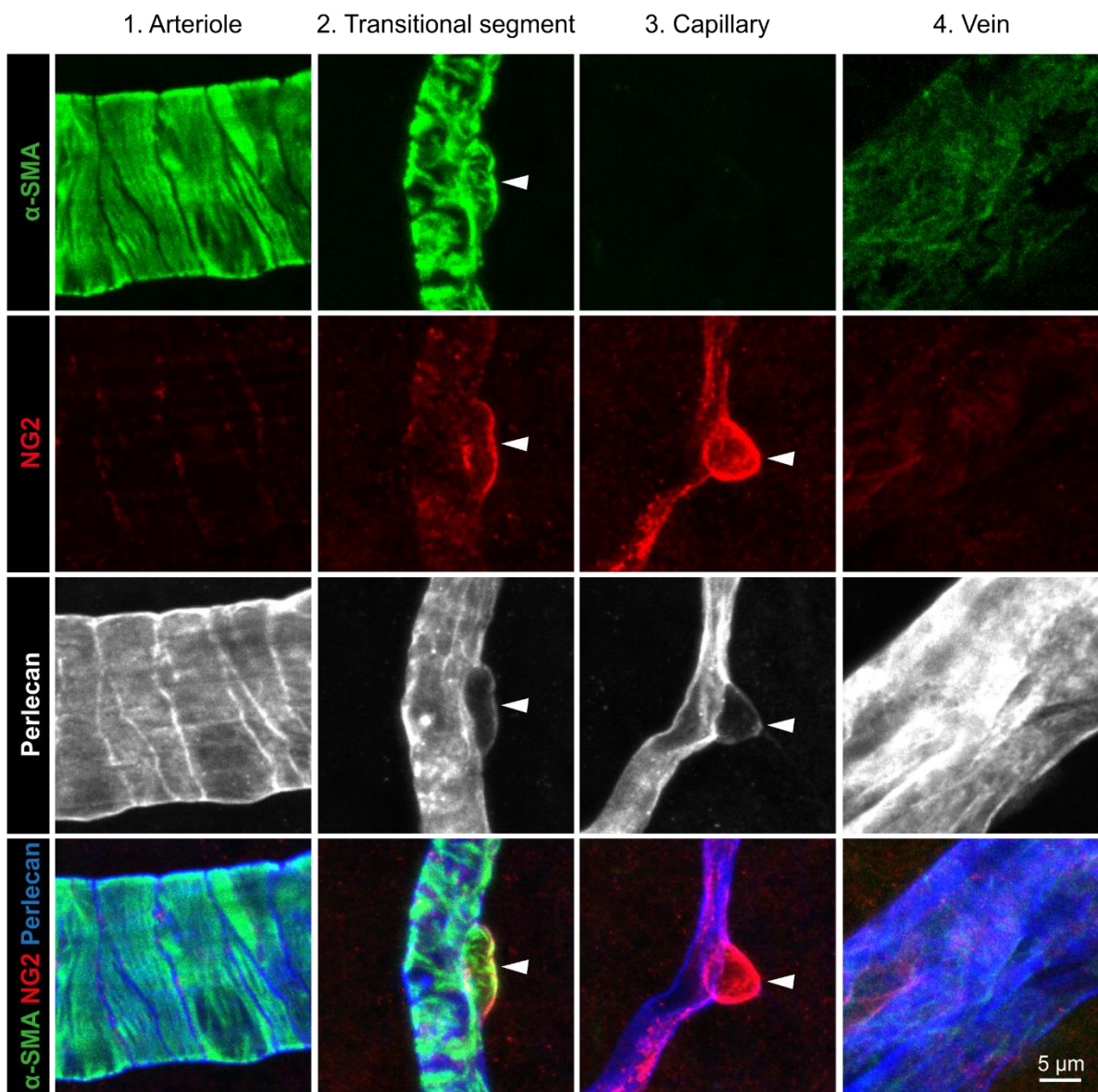
16
17

18

1 **FIGURES and LEGENDS**

A
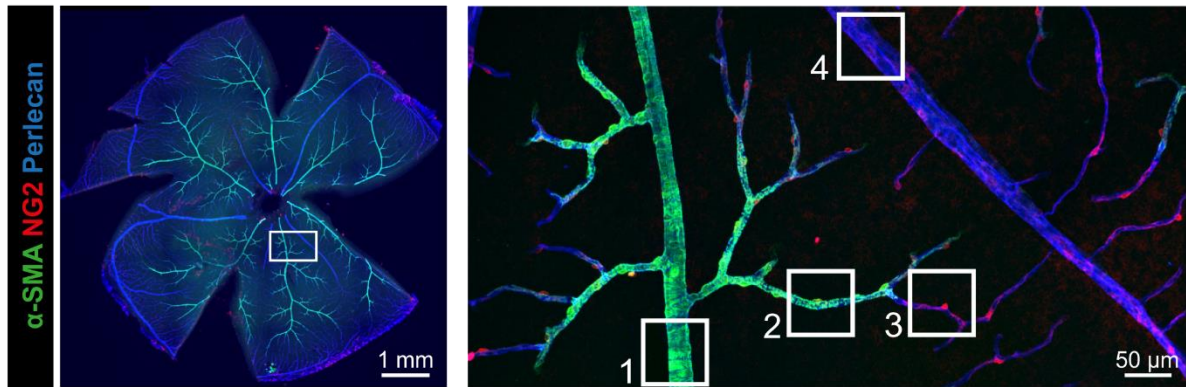
B

2 Figure 1

1   **Figure 1. Heterogeneity of mural cells in retinal vessels.** Confocal pictures of adult mouse

2   retina immunostained for α-SMA, NG2 and perlecan. **A**. Whole flat mounted retina (left

3   panel). Higher magnification of the boxed region (right panel). **B**. Higher magnification

4   pictures of the boxed regions numbered in A, showing SMCs in arterioles (1), transitional

5   cells in transitional segments (2), pericytes in capillaries (3) and SMCs in veins (4).

6   Arrowheads show protruding cell body in transitional segments and capillaries. Scale bars: 1

7   mm (A, left), 50 μm (A, right) and 5 μm (B).

8

9
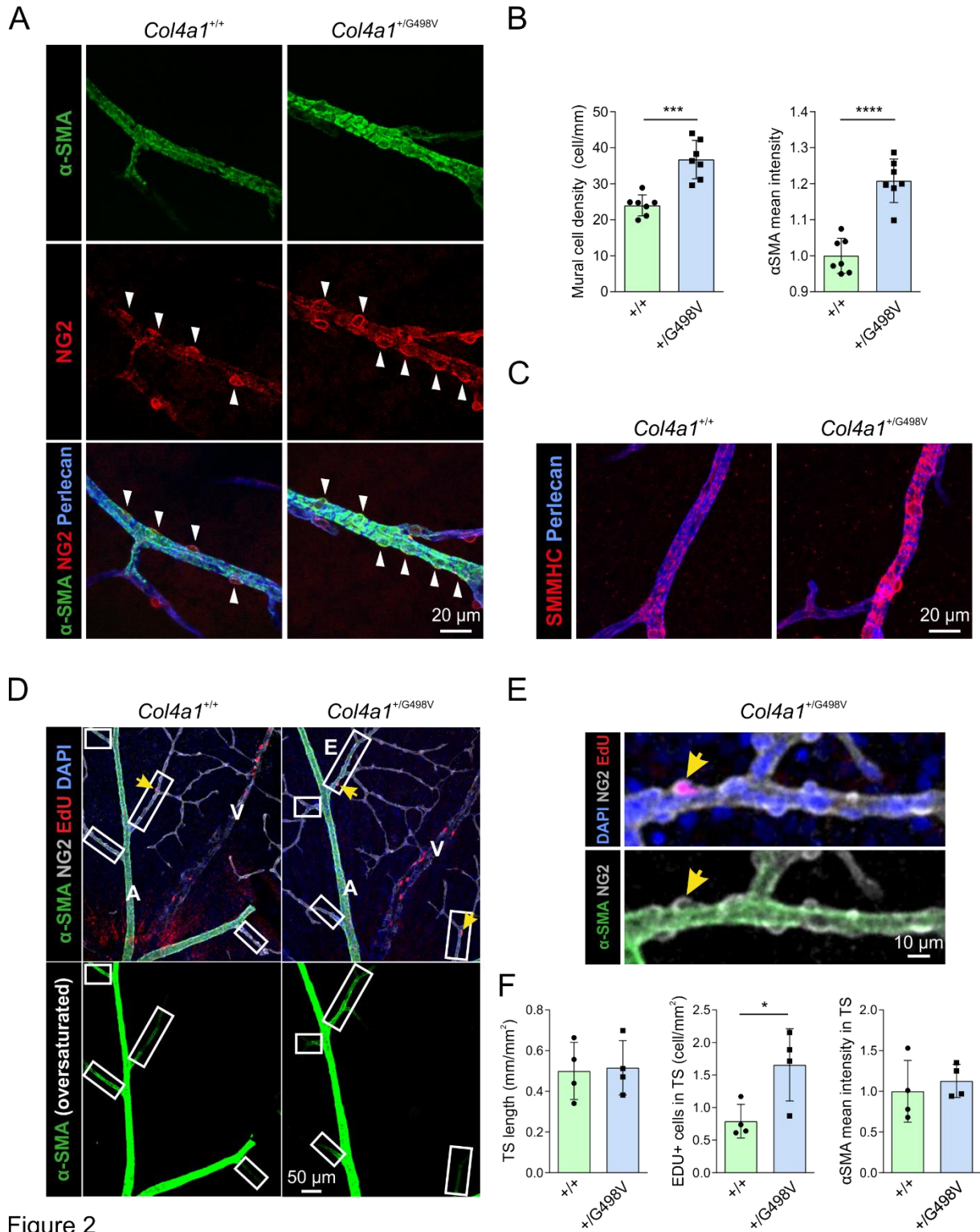
1   Figure 2

2

3   **Figure 2. TS in *Col4a1^+/G498V* retina are hypermuscularized in adult mice and exhibit**

4   **increased mural cell proliferation during the post-natal maturation of the retinal**

5   **vasculature. A**. Representative confocal pictures of retinal TS from *Col4a1^+/+* and

34

1 *Col4a1*^{+/G498V} mice aged 6 months stained for α-SMA, NG2 and perlecan. TS in mutant mice

2 exhibit greater α-SMA fluorescence intensity and an increased number of transitional cells

3 (arrowheads). **B**. Quantification of mural cell density and α-SMA mean fluorescence intensity

4 in retinal TS of *Col4a1*^{+/+} and *Col4a1*^{+/G498V} mice at 6 months (n=7 mice per group). ***

5 *P*=0.0001 **** *P*<0.0001 by Student's t-test. **C**. Representative confocal pictures of TS of

6 *Col4a1*^{+/+} and *Col4a1*^{+/G498V} mice at 6 months stained for SMMHC and perlecan showing

7 higher SMMHC expression in mutant vessels. **D.** Representative confocal images of retinal

8 arterioles (A) and TS (white boxes) of *Col4a1*^{+/+} and *Col4a1*^{+/G498V} mice aged 10 days,

9 stained for EdU incorporation (4 hours) together with α-SMA, NG2, and DAPI— Shown are

10 oversaturated images of α-SMA staining to better visualize TS (bottom panel). Yellow arrows

11 depict proliferating mural cells in TS. Note the sustained cell proliferation in wildtype and

12 mutant veins (V). **E.** Higher magnification views of the boxed area in D showing a

13 proliferating mural cell in the TS of a *Col4a1*^{+/G498V} mouse (yellow arrow) **F**. Quantification

14 of the total length of TS (*P*=0.8746) stained by α-SMA, mural cell proliferation in TS (*

15 *P*=0.0298) and α-SMA mean fluorescence intensity in TS (*P*=0.5753). Data were analyzed by

16 Student's t-test (n=4 mice per group). Scale bars: 20 µm (A, C), 50 µm (D) and 10 µm (E).

17

18
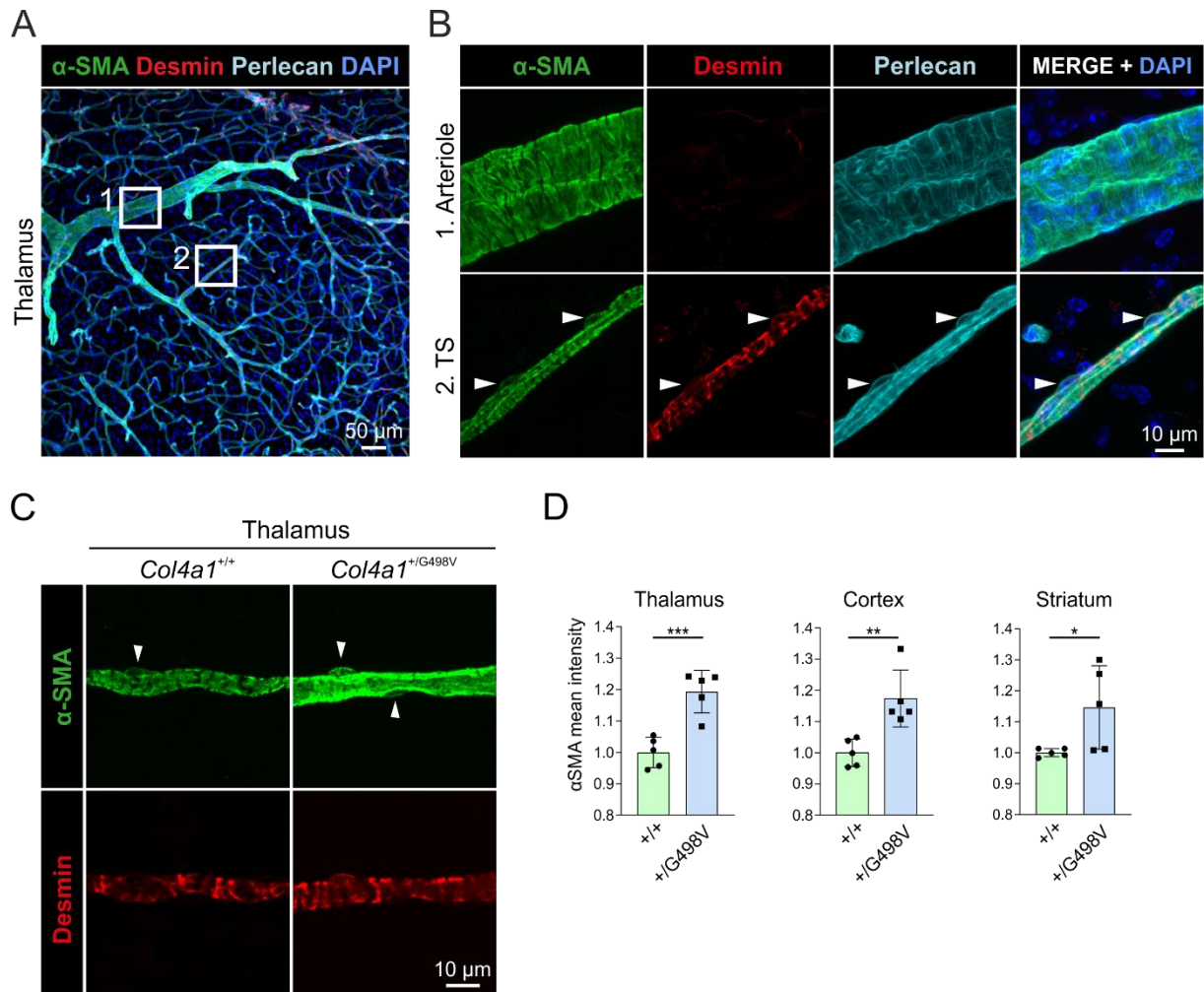
Figure 3

Figure 3. TS are present in the brain vasculature and are hypermuscularized in

Col4a1^{+/G498V} **mice. A, B** Representative confocal pictures of an adult wildtype mouse brain

immunostained for α-SMA, desmin, perlecan and Dapi. **A**. Low magnification view of a

vascular tree. **B**. Higher magnification pictures of the boxed regions numbered in A, showing

SMCs in arterioles (1), and transitional cells in TS (2). Arrowheads point to the protruding

cell body of transitional cells in the TS, containing the nucleus. **C**. Representative confocal

pictures of TS in the thalamus from *Col4a1^{+/+}* and *Col4a1^{+/G498V}* mice aged 6 months stained

for α-SMA and desmin, showing increased α-SMA immunoreactivity in mutant TS.

Arrowheads point to cell nucleus of transitional cells. **D**. Quantification of α-SMA mean

fluorescence intensity in TS of *Col4a1^{+/+}* and *Col4a1^{+/G498V}* mice aged 6 months in the
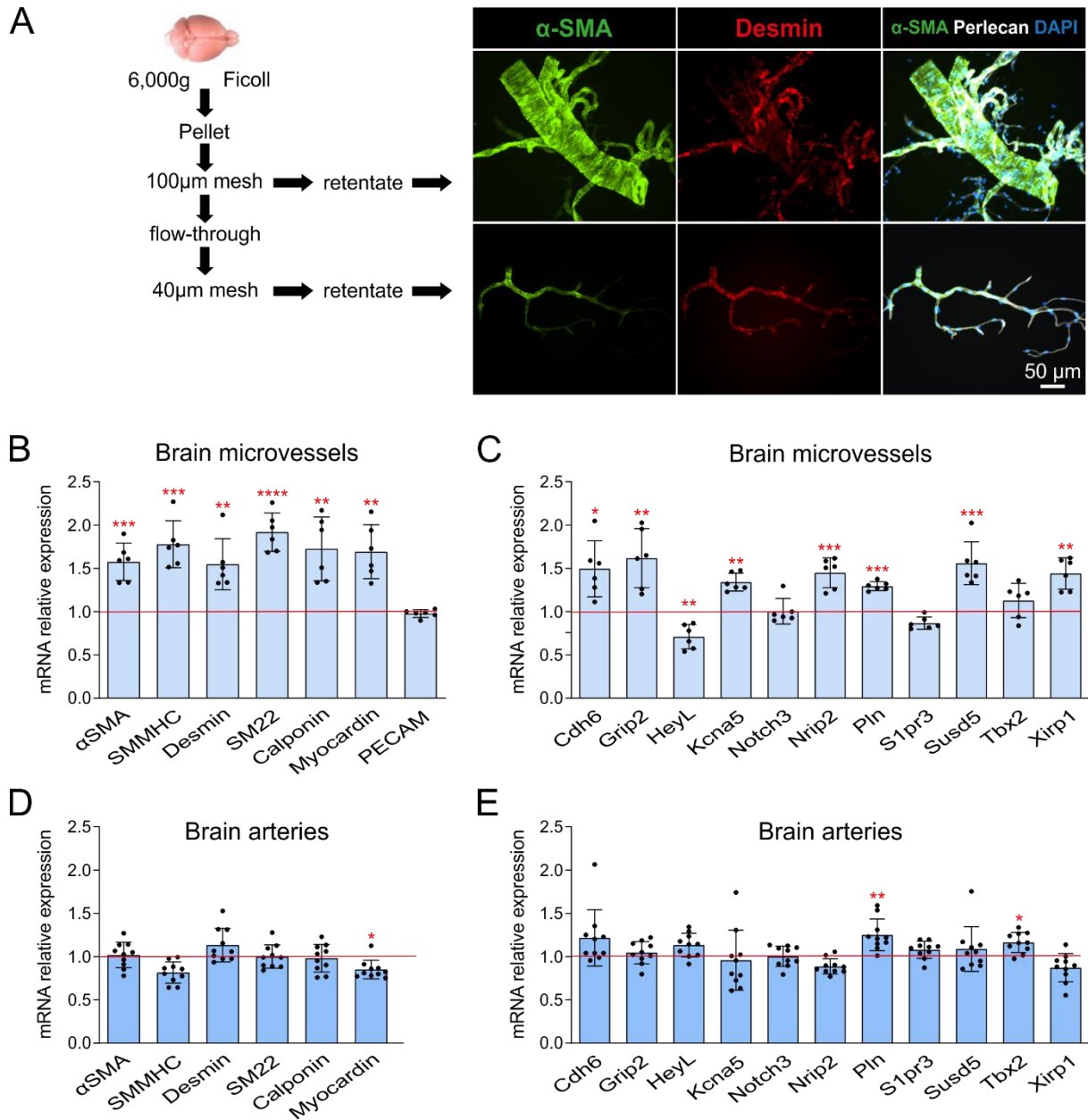
1   thalamus (*** *P*=0.0008), cortex (** *P*=0.005) and striatum (* *P*=0.0422). Data were

2   analyzed by Student's t-test (n=5 mice per group). Scale bars: 50 µm (A) and 10 µm (B,C).

3

4

5

6

1   Figure 4

2   **Figure 4. Gene expression level of SMC genes and Notch3 target genes in brain**

3   **microvessels and brain arteries of *Col4a1*^{+/+} and *Col4a1*[+/G498V] mice. A**. Microvessels were

4   prepared from mouse brain by homogeneization and centrifugation into Ficoll solution as

5   described in the supplementary method section. Vessel preparations were then fractionated

6   successively through 100 and 40 μm nylon meshes. Pictures show vessels retained on each

7   nylon mesh (100 and 40 μm-fractions) stained for α-SMA, desmin, perlecan and DAPI.

8   Arterioles (bright for α-SMA and low for desmin) were retained in the 100 μm-fraction and

40 µm-fractions were enriched in TS (bright for α-SMA and desmin) and capillaries. **B, C**. Relative mRNA levels of smooth muscle genes (**B**) and Notch3 target genes (**C**) measured by quantitative RT-PCR on 40 µm-fractions prepared from *Col4a1*$^{+/+}$ and *Col4a1*$^{+/G498V}$ adult mice (n=6 mice per group). Data are reported as a fold change over control mice and analyzed by Student's t-test. α-SMA (*** P=0.0007), SMMHC (*** P=0.0002), Desmin (** P=0.0018), SM22 (**** P<0.0001), Calponin (** P=0.0041), Myocardin (** P=0.0013), PECAM (P=0.4934), Cdh6 (* P=0.0117), Grip2 (** P=0.0048), HeyL (** P=0.0035), Kcna5 (** P=0.0060), Notch3 (P=0.9697), Nrip2 (*** P=0.0002), Pln (*** P=0.0007), S1pr3 (P=0.0530), Susd5 (*** P=0.001), Tbx2 (P=0.1972), and Xirp1 (** P=0.0085). **D, E**. Relative mRNA levels of smooth muscle genes (**D**) and Notch3 target genes (**E**) measured by quantitative RT-PCR in dissected brain arteries from *Col4a1*$^{+/+}$ and *Col4a1*$^{+/G498V}$ adult mice (n=10 mice per group). Data are reported as a fold change over control mice and analyzed by Student's t-test. α-SMA (P=0.7811), SMMHC (P=0.0506), Desmin (P=0.1680), SM22 (P=0.9903), Calponin (P=0.8291), Myocardin (* P=0.0407), Cdh6 (P=0.0609), Grip2 (P=0.5982), HeyL (P=0.1397), Kcna5 (P=0.8060), Notch3 (P=0.9669), Nrip2 (P=0.1677), Pln (** P=0.0062), S1pr3 (P=0.4643), Susd5 (P=0.4996), Tbx2 (* P=0.0309), and Xirp1 (P=0.2664). Scale bar: 50 µm (A).
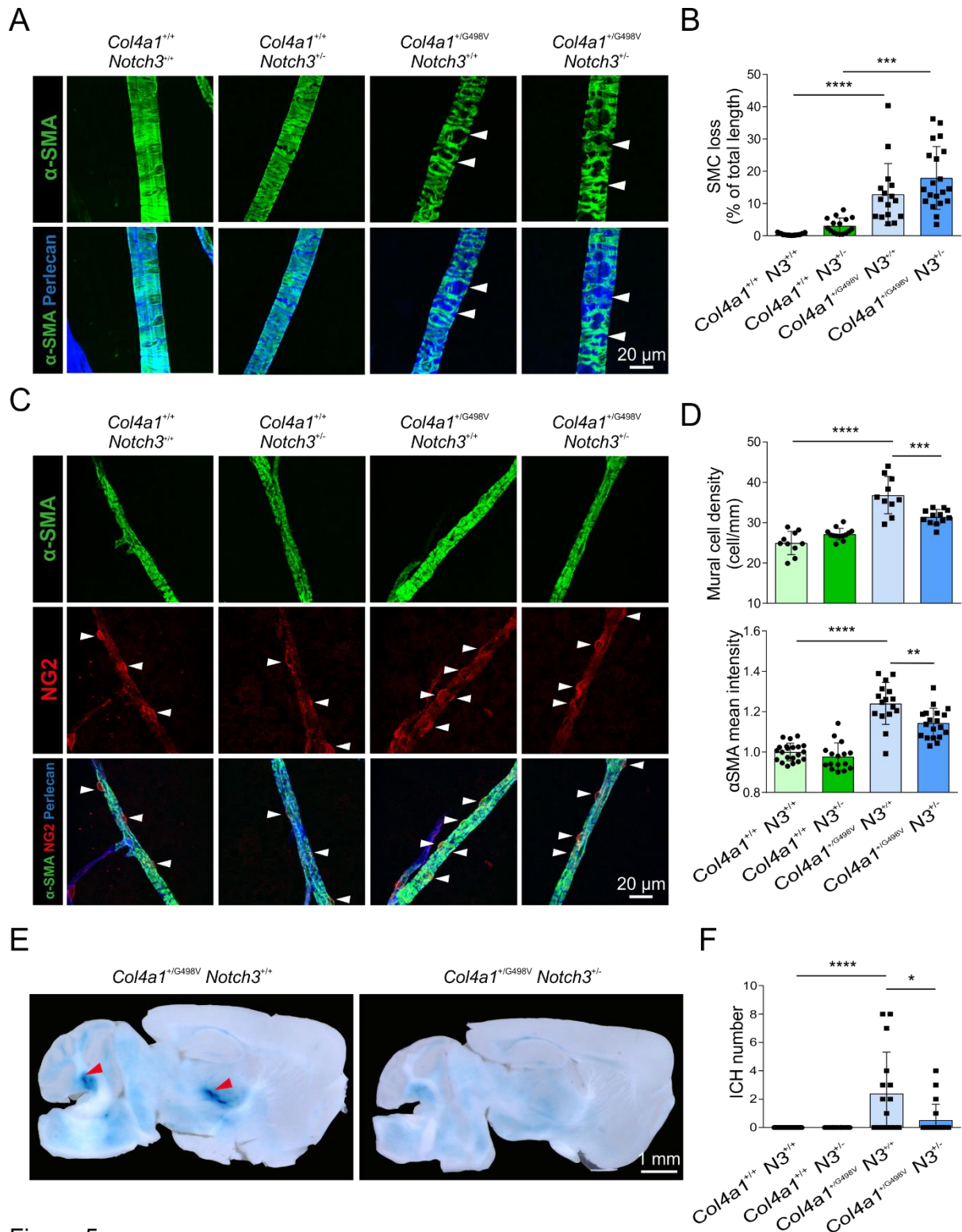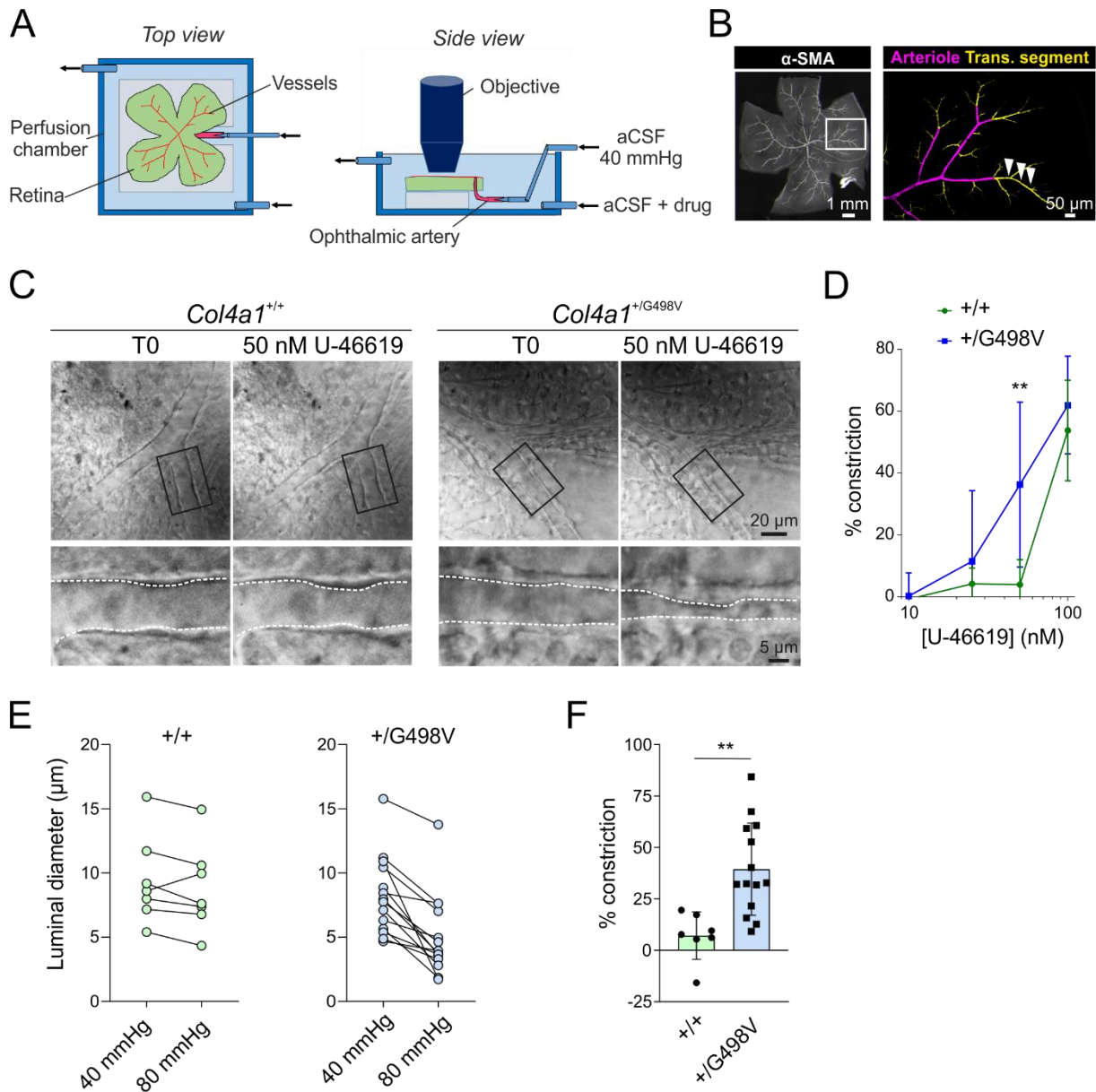
Figure 5

1

Figure 5. Genetic reduction of Notch3 attenuates the hypermuscularization of TS in the

retina and protects *Col4a1* mutant mice against ICH. *Col4a1*[+/G498V] mice were crossed

1   with *Notch3*$^{+/-}$ mice and issued mice of the four following genotypes were screened for

2   microvascular lesions and ICHs at 6 months of age: *Col4a1*$^{+/+}$, *Notch3*$^{+/+}$; *Col4a1*$^{+/+}$,

3   *Notch3*$^{+/-}$; *Col4a1*$^{+/G498V}$, *Notch3*$^{+/+}$ and *Col4a1*$^{+/G498V}$, *Notch3*$^{+/-}$. **A**. Representative confocal

4   pictures of retinal arterioles stained for α-SMA and perlecan, showing SMC loss

5   (arrowheads). **B**. Quantification of SMC loss in retinal arterioles showing no significant

6   difference between *Col4a1*$^{+/G498V}$, *Notch3*$^{+/+}$ and *Col4a1*$^{+/G498V}$, *Notch3*$^{+/-}$ mice (from left to

7   right n=21, 16, 16 and 20 mice). Data were analyzed with Kruskal-Wallis and Dunn's post-

8   hoc test. *** *P*=0.0005 **** *P* < 0.0001. **C**. Representative confocal pictures of retinal TS

9   stained for α-SMA, NG2 and perlecan. Arrowheads show cell bodies of transitional cells. **D**.

10   Quantification of mural cell density (from left to right n=10, 13,10 and 12 mice) and α-SMA

11   mean fluorescence intensity (from left to right n=21, 16,16 and 20 mice) in TS showing a

12   significant reduction in mural cell density and α-SMA intensity in *Col4a1*$^{+/G498V}$ *Notch3*$^{+/-}$

13   mice compared to *Col4a1*$^{+/G498V}$ *Notch3*$^{+/+}$ mice. Data were analyzed by one-way ANOVA

14   and Tukey's post-hoc test. Mural cell density *** *P*=0.0004 ,**** *P*<0.0001. α-SMA

15   intensity **** *P*<0.0001. **E.** Representative images of sagittal brain sections stained for

16   hemosiderin. Arrowheads depict deep ICHs. **F**. Quantification of the number of ICH showing

17   a significant decrease in ICH number in *Col4a1*$^{+/G498V}$, *Notch3*$^{+/-}$ mice compared to

18   *Col4a1*$^{+/G498V}$, *Notch3*$^{+/+}$ mice (from left to right n=21, 16,16 and 20 mice). Data were

19   analyzed by Kruskal-Wallis and Dunn's post-hoc test. * *P*=0.020, **** *P*<0.0001. Scale bars:
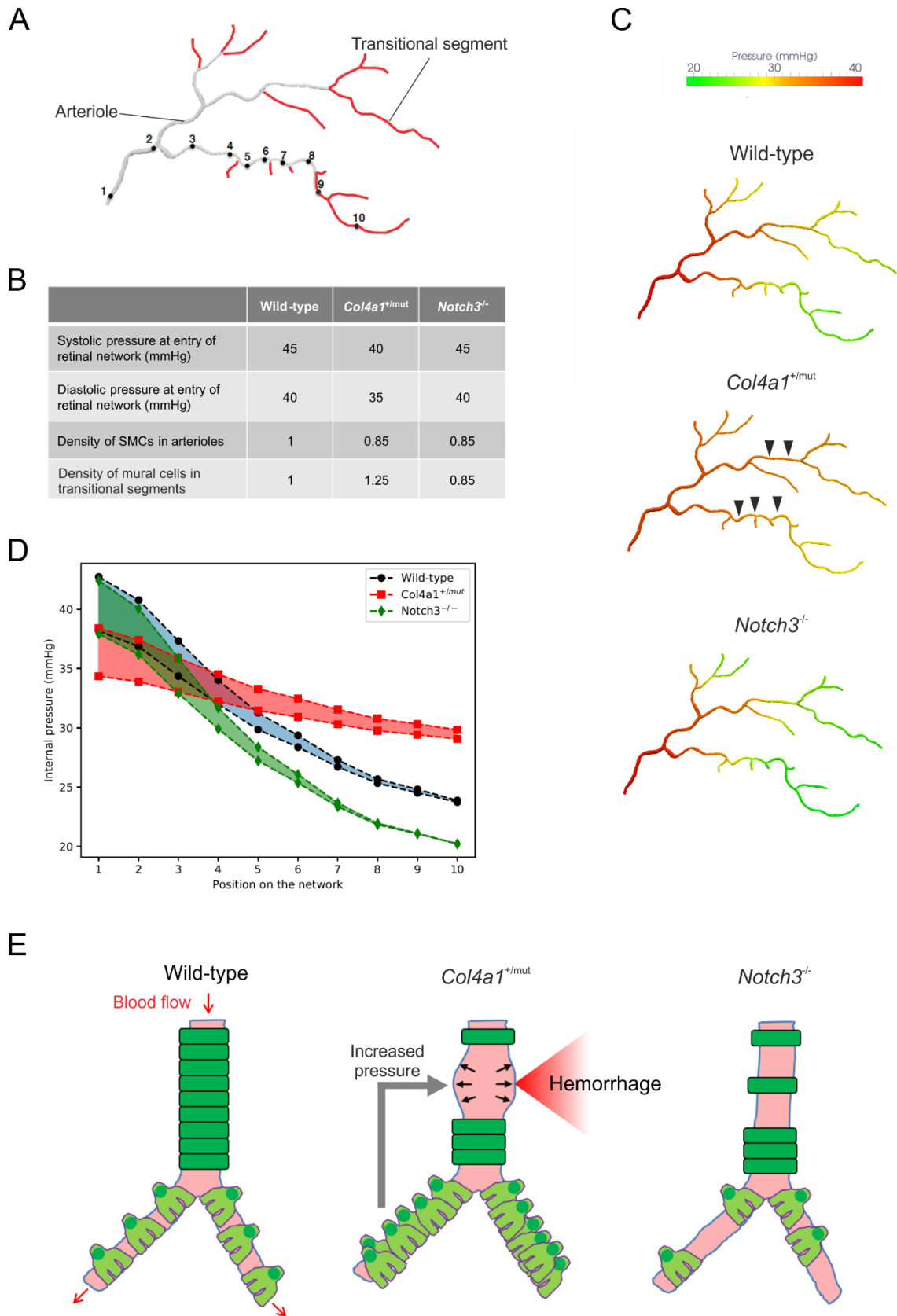
20   20 μm (A, C) and 1 mm (E).

21

22

Figure 6. Agonist and pressure-induced contractile responses are greater in TS of

Col4a1[+/G498V] **mice. A**. Experimental setup to analyze contractility and tone of the TS in retina

explants. The retina was dissected with the ophthalmic artery and pinned on a silicon platform

with the vessels facing upwards and immerged in a perfusion chamber filled with circulating

aCSF at 37°C. To pressurize retinal vessels, ophthalmic artery was cannulated on a

micropipette fed with a gravity column of CSF at 40 mmHg. Changes in vessel diameters

were observed using a water immersion 40X objective. **B**. Whole retina (left panel).

Schematic depicting TS (yellow, arrowheads) and arterioles (purple) analyzed in these experiments (right panel)— noting that the capillaries are not depicted in this schematic. **C.** Differential interference contrast images of TS from *Col4a1*$^{+/+}$ and *Col4a1*$^{+/G498V}$ mice aged 6 months before (T0) and after addition of 50 nM thromboxane agonist U-46619 to the perfusion chamber. Bottom pictures show higher magnification view of boxed regions. Dashed white lines delineate the vessel wall. **D**. Dose response curve showing increased constriction of *Col4a1*$^{+/G498V}$ TS in response to U-46619 (n=5 *Col4a1*$^{+/+}$ and 9 *Col4a1*$^{+/G498V}$ mice). **E.** Decreasing diameters of individual TS following 40 mmHg to 80 mmHg pressure increase at the ophthalmic artery **F.** Increased pressure-induced constriction in *Col4a1*$^{+/G498V}$ TS, shown as percent constriction (relative to 40 mmHg diameter, n=7 vessels from 3 *Col4a1*$^{+/+}$ mice and n=14 vessels from 5 *Col4a1*$^{+/G498V}$ mice). Data were analyzed by repeated measure 2-way ANOVA and Bonferroni's multiple comparison test (panel D, ** P=0.0051), or Student's t-test (panel F, ** P=0.0021). Scale bars: 1mm (B, left), 50 µm (B, right), 20 µm (C, top) and 5 µm (C, bottom).

A

Transitional segment

Arteriole

B

	Wild-type	Col4a1+/mut	Notch3-/-
Systolic pressure at entry of retinal network (mmHg)	45	40	45
Diastolic pressure at entry of retinal network (mmHg)	40	35	40
Density of SMCs in arterioles	1	0.85	0.85
Density of mural cells in transitional segments	1	1.25	0.85

C

Pressure (mmHg)
20   30   40

Wild-type

Col4a1+/mut

Notch3-/-

D

Internal pressure (mmHg) vs Position on the network

- Wild-type
- Col4a1+/mut
- Notch3-/-

E

Wild-type   Col4a1+/mut   Notch3-/-

Blood flow ↓

Increased pressure   Hemorrhage

Figure 7

Figure 7. Computational modeling predicts that excessive muscularization of the TS increases intravascular pressure in the upstream arteriolar segment. A. Geometry of the human retinal vascular tree used for mathematical modeling. Arterioles are depicted in grey and transitional segments in red. **B**. Input parameters used for mathematical modeling. **C**. Color-coded representation of systolic intravascular pressures along the retinal vascular tree simulated with the model in wild-type (top), *Col4a1* mutant (middle) and *Notch3*^{-/-} (bottom) mice, showing that pressure is elevated in terminal arterioles and TS of *Col4a1* mutant mice (arrowheads) but reduced in *Notch3*^{-/-} mice. **D**. Graph showing simulated systolic and diastolic pressures at 10 different points on the vascular tree represented in A. **E**. Proposed working model of the mechanism of arteriolar wall rupture in *Col4a1* mutant mice.
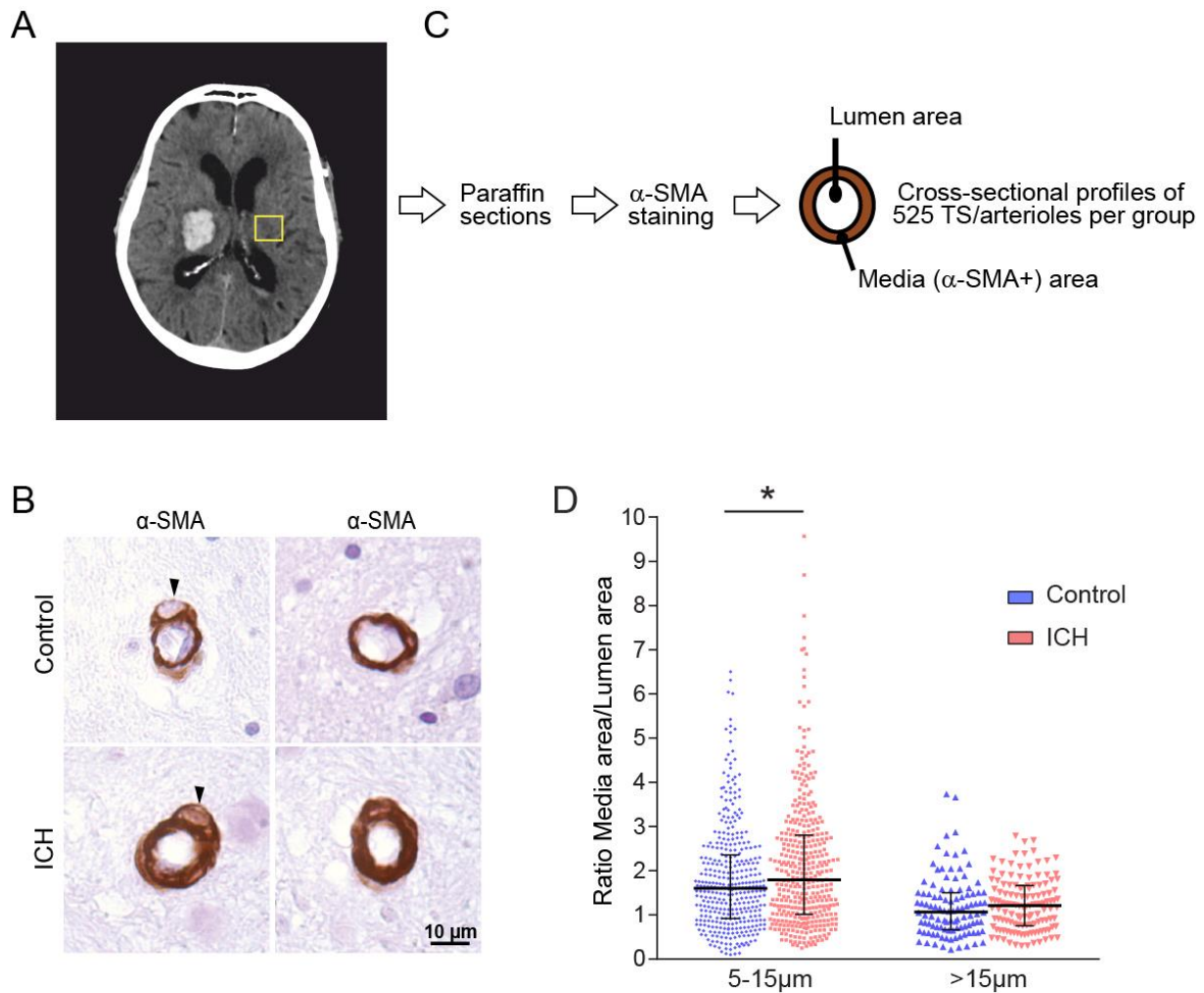
Figure 8

Figure 8. Hypermuscularization of the TS in humans with deep ICH. A. Representative

image of a CT-scan showing a deep ICH in the left thalamus. Brain tissue was sampled after

death in the contralateral basal ganglia for immuno-histochemistry (boxed region) and

embedded in paraffin. **B**. Representative images of cerebral TS (basal ganglia) stained for α-

SMA showing an hypermuscularization in ICH patients. Arrowheads point to transitional cell

bodies. **C**. Schematic of the methodology used to quantify vessel wall remodeling. Cross-

sectional profiles of 525 randomly selected arterioles/TS were analyzed in each group. **D**.

Ratio of the vessel area stained for α-SMA (media) over the area of the lumen in cerebral

46

1   arterioles/TS from control and ICH patients. Vessels were stratified into two categories

2   according to their lumen diameter (5 to 15 µm, TS and > 15 µm, arterioles). From left to right

3   n = 368 and 382 TS (5-15µm), 106 and 128 arterioles (>15µm) analyzed. Data are presented

4   as scatter plots with median value and first/third quartiles. Data were analyzed by Kruskal-

5   Wallis and Dunn's post-hoc test. * *P*=0.016 Scale bar: 10 µm (B).

6